ADVANCED FUNCTIONAL MATERIALS
www.afm-journal.de

$HPbI_3$: A New Precursor Compound for Highly Efficient Solution-Processed Perovskite Solar Cells

*Feng Wang, Hui Yu, Haihua Xu, and Ni Zhao**

Recently, there have been extensive research efforts on developing high performance organolead halide based perovskite solar cells. While most studies focused on optimizing the deposition processes of the perovskite films, the selection of the precursors has been rather limited to the lead halide/methylammonium (or formamidium) halide combination. In this work, we developed a new precursor, $HPbI_3$, to replace lead halide. The new precursor enables formation of highly uniform formamidium lead iodide ($FAPbI_3$) films through a one-step spin-coating process. Furthermore, the $FAPbI_3$ perovskite films exhibit a highly crystalline phase with strong (110) preferred orientation and excellent thermal stability. The planar heterojunction solar cells based on these perovskite films exhibit an average efficiency of 15.4% and champion efficiency of 17.5% under AM 1.5 G illumination. By comparing the morphology and formation process of the perovskite films fabricated from the formamidium iodide (FAI)/$HPbI_3$, FAI/PbI_2, and FAI/PbI_2 with HI additive precursor combinations, it is shown that the superior property of the $HPbI_3$ based perovskite films may originate from 1) a slow crystallization process involving exchange of H^+ and FA^+ ions in the PbI_6 octahedral framework and 2) elimination of water in the precursor solution state.

1. Introduction

Hybrid organic–inorganic perovskites have recently emerged as a promising candidate for the next-generation solar cells with high efficiency, light weight, and low-temperature processability.[1] A general chemical formula of the perovskites can be written as ABX_3, where A is an organic cation (e.g., $CH_3NH_3^+$ or $HC(NH_2)_2^+$), B is a metal cation (Pb^{2+} or Sn^{2+}), and X is a halide anion.[2] The ABX_3 perovskite materials can be produced by mixing the AX and BX_2 precursors in solution or vapor phase, followed by thermal annealing. The fabrication process of the ABX_3 perovskite thin films is of particular concern for highly efficient solar cells, since it directly determines the uniformity and crystallinity of the perovskite layer. Four methods, including one-step solution-coating,[3] vapor-assisted deposition,[4] sequential deposition,[5] and dual-source evaporation,[6] have been developed to produce ABX_3 perovskite films for high efficiency solar cells. Among these methods, the solution-coating process that involves only the deposition of the $AX:BX_2$ precursor mixture is the simplest process and hence attractive for future industrialization.[7] However, the one-step solution-processed perovskite films often encounter the problems of film non-uniformity and incomplete coverage.[5a,8] Accordingly, attempts have been made to control the crystallization process of perovskite to improve the film quality. For example, Snaith et al. found that the use of methylammonium chloride (CH_3NH_3Cl) precursor could slow down the formation process of $CH_3NH_3PbI_3$ (also referred as $CH_3NH_3PbI_{3-x}Cl_x$) and thus improve the film morphology and extend the carrier's lifetime.[1,9] Seok et al. deposited the perovskite films from a mixed solvent of γ-butyrolactone and dimethylsulphoxide (DMSO), followed by toluene drop-casting.[10] This method produces highly uniform and dense perovskite layers via a "CH_3NH_3I–PbI_2–DMSO intermediate phase" and results in solar cells with a power-conversion efficiency (PCE) of 16.2% and no hysteresis.[10,11] Meanwhile, Spiccia et al. demonstrated that exposure of $CH_3NH_3PbI_3$ precursor films to chlorobenzene could be an alternative approach to facilitate the crystallization of perovskites.[12] In both methods, the starting time and duration of introducing the inert solvent (e.g., toluene and chlorobenzene) to the precursor film is critical to the quality of the final product, therefore increasing the complexity of device fabrication.

Besides crystallization, precursor solubility is another processing parameter that affects the morphology of perovskite films. It has been shown that the solubility of $PbCl_2$ in DMF is greatly improved by introducing 1,8-diiodooctane solvent additive; this approach facilitates homogenous nucleation during crystallization of $CH_3NH_3PbI_{3-x}Cl_x$ perovskite films and subsequently leads to an increase of solar cell PCE from 9.0% to 11.8%.[13] Apart from methylammonium lead iodide ($MAPbI_3$), formamidium lead iodide ($FAPbI_3$) perovskite has recently received much attention due to its extended absorption range and excellent charge transport properties.[14] In order to produce uniform and continuous $FAPbI_3$ perovskite films, it is necessary to add a small amount of hydroiodic (HI) acid to the precursor solution.[14a] However, the influence of HI and water (present in the HI acid) on the formation of perovskite remains unclear.

Dr. F. Wang, H. Yu, Dr. H. H. Xu, Prof. N. Zhao
Department of Electronic Engineering
The Chinese University of Hong Kong
New Territories, Hong Kong
E-mail: nzhao@ee.cuhk.edu.hk
Prof. N. Zhao
Shenzhen Research Institute
The Chinese University of Hong Kong
New Territories, Hong Kong

DOI: 10.1002/adfm.201404007

Despite the extensive studies on optimizing the deposition processes of perovskite films, the selection of the precursors is rather limited to the PbI_2 (or $PbCl_2$) based material systems. In this work, we present a new precursor compound, $HPbI_x$, for solution-processed fabrication of high-performance perovskite solar cells. The precursor is synthesized by reacting PbI_2 with HI and shows excellent solubility in DMF. It allows formation of highly uniform, dense, and thick films of $FAPbI_3$ perovskite through one-step spin-coating of $HPbI_x$/formamidine iodide (FAI) precursor solution in DMF. As compared to the $FAPbI_3$ films fabricated from PbI_2 based precursor systems, the $HPbI_x$/FAI produced $FAPbI_3$ films exhibit much purer crystalline phase with strong (110) preferred orientation. Such high crystallinity benefits from a slow crystallization process involving exchange of H^+ and FA^+ ions in the PbI_6 octahedral framework, as well as elimination of water in the precursor solution state. The $FAPbI_3$ films are integrated in a simple planar solar cell structure and yield an average efficiency of 15.4% and champion efficiency of 17.5%, calculated from current–voltage scans under AM 1.5 illumination.

2. Results and Discussion

2.1. Characterizations of $HPbI_3$

The $HPbI_x$ compound was formed through a reaction of PbI_2 and HI in DMF (see "Experimental Section" for the detailed synthesis procedure) and appears in light yellow in the powder form (Figure S1, Supporting Information). The atomic ratio of I in the $HPbI_x$ compound was first measured by thermogravimetric analyzer (TGA). As shown in **Figure 1**a, the compound starts to decompose at 240 °C, accompanied by the release of HI. Such high temperature implies the formation of chemical bonds between HI and PbI_2 during the reaction. The loss fraction from 240 to 345 °C is ≈23.7% by weight, indicating the molar ratio of PbI_2 to HI in the compound is ≈1:1.1. X-ray photoelectron spectroscopy (XPS) measurement further confirms the molar ratio of PbI_2 to HI to be around 1:1 (Figure 1b). These results suggest that the $HPbI_x$ compound is likely to adopt a chemical formula of $HPbI_3$, although we cannot exclude the possibility of the existence of a very small amount of other lead iodide phases in the powder. Note that there have been reports on alkali lead iodides with a chemical structure of $MPbI_3$, M_2PbI_4, or M_4PbI_6 and trihalogermanes with a chemical structure of $HGeX_3$.[15] Interestingly, the solubility of $HPbI_3$ in DMF is up to ≈2.5 M at room temperature. As shown in Figure 2b, 2.0 M $HPbI_3$ could be dissolved in DMF within 5 min under stirring; in contrast, 2.0 M PbI_2 in DMF remains as a slurry even after 2 days' stirring at room temperature.

The crystal structure of the $HPbI_3$ compound was analyzed using x-ray diffraction (XRD) measurement and compared with the structure of PbI_2. As shown in Figure 1c, the XRD peak of PbI_2 at 12.8° corresponds to a layered structure with the interlayer spacing of 6.98 Å along the z axis. Within each PbI_2 layer, Pb–I octahedrons are connected in an edge-sharing fashion along both the x and y axes (**Figure 2**).[16] $HPbI_3$ adopts a similar XRD pattern with the low angle peak shifted to 11.5°, indicating an increased interlayer distance in $HPbI_3$ as compared to PbI_2. Such expansion of the interlayer

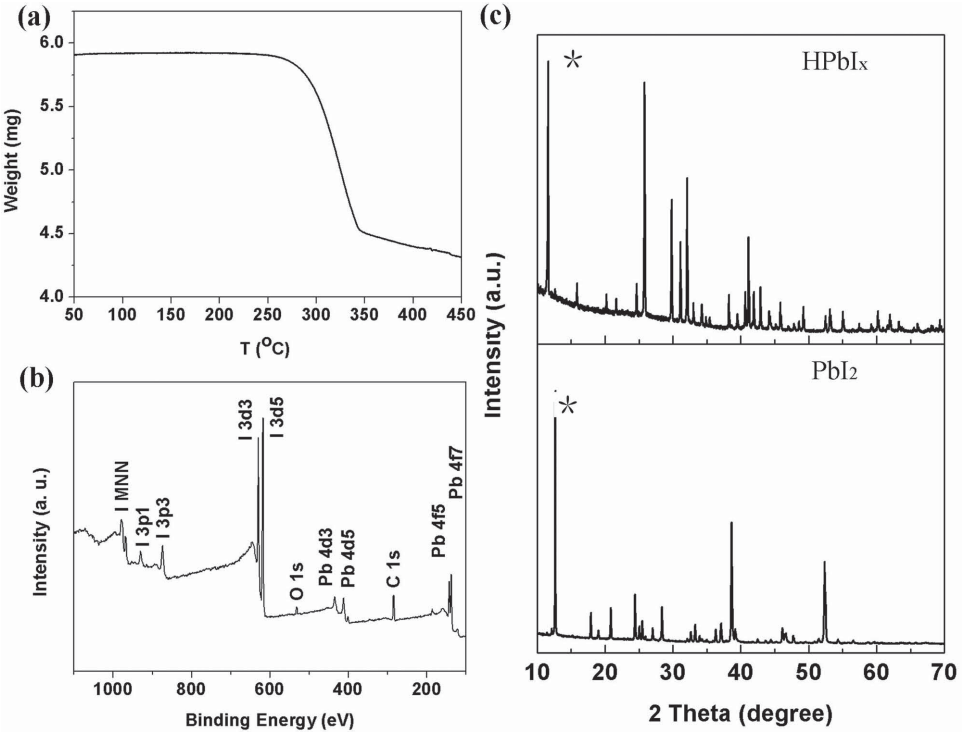

Figure 1. a) TGA spectrum and b) XPS spectrum of $HPbI_x$. c) XRD patterns of $HPbI_3$ and PbI_2. * Highlights the XRD peaks corresponding to the (001) plane of the layered structures.

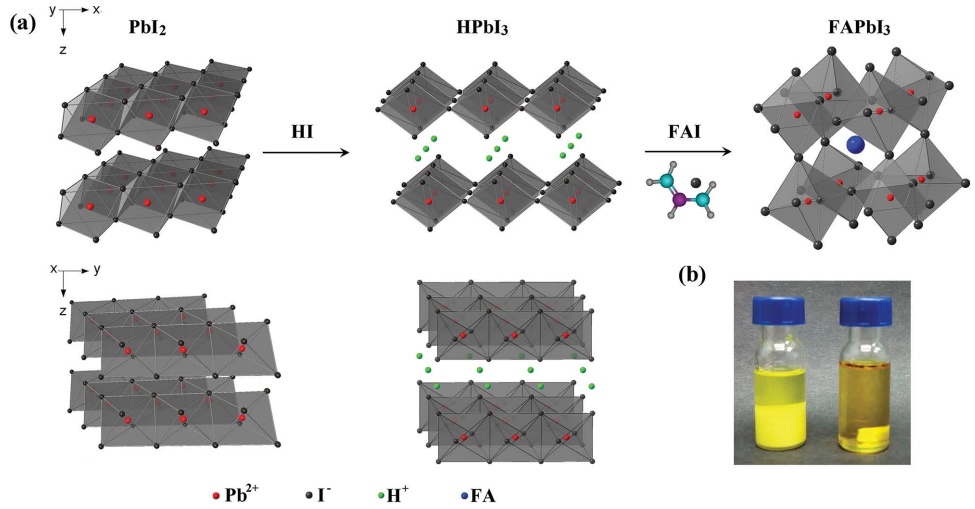

Figure 2. a) Schematic illustration of the configurations of PbI_2, $HPbI_3$, and $FAPbI_3$. b) Solubility comparison of PbI_2 (left) and $HPbI_3$ (right) in DMF. Both solutions have a concentration of 2.0 M and have been stirred for 24 h.

spacing could originate from the intercalation of H^+ ions. Similar phenomenon was also observed in the MAI–PbI_2–DMSO complex.[10] Note that due to the coordination requirement between the iodine and lead ions in $HPbI_3$, the edge-sharing configuration of the Pb–I octahedrons should be changed to corner sharing along the *x*-axis. The detailed analysis of the crystal structure of $HPbI_3$ can be found in the Supporting Information.

2.2. Properties of Perovskite Films

We now turn to discuss the formation process of $FAPbI_3$ perovskite using different precursor combinations. We compare the perovskite films formed from FAI/$HPbI_3$, FAI/PbI_2, and FAI/PbI_2 with 5 vol% HI (57 wt% in H_2O) additive, respectively. (Note that the HI percentage is optimized for solar cells. See more details in Table S1, Supporting Information.) The XRD patterns of the films (**Figure 3**) confirm that all precursor combinations can be converted to $FAPbI_3$ perovskite phase; however, the FAI/$HPbI_3$ formed perovskite film exhibits the highest crystallinity with strong (110) preferred orientation (corresponding to the 13.9° peak). To understand the origin of such difference, we further investigated the perovskite formation process as a function of annealing time (Figure S2, Supporting Information). The results indicate that the complete conversion to perovskite from FAI/PbI_2 and FAI/PbI_2 with HI need ≈20 min and 5 min, respectively. On the other hand, the FAI/$HPbI_3$ combination retards the reaction process to 40 min. It is proposed that the formation of $FAPbI_3$ is driven by the intercalation of FAI into the interlayer of PbI_2.[17] In the case of $FAPbI_3$ formed from the $HPbI_3$ network, the intercalation process may be hindered by the hydrogen bonds between the H^+ ions and Pb–I octahedrons. Besides, the release of excess I^- might also affect the crystallization kinetics. Accordingly, the perovskite formation process is slowed down. It has been shown previously for $MAPbI_3$ perovskites that a slow reaction/crystallization process is beneficial for the formation of dense films with high crystallinity.[11,18] The same principle could be applied to the $FAPbI_3$ system. Furthermore, comparing the DMF solution of $HPbI_3$/FAI and PbI_2/FAI with HI additive, the former brings in much higher concentration of H^+ and I^- with no trace amount of H_2O in the precursor solution state. The elimination of H_2O is beneficial for the film quality as H_2O is unfavorable for the perovskite formation with oriented crystallinity. We also note that among the three $FAPbI_3$ samples formed from different precursors, the FAI/$HPbI_3$ produced sample shows the best thermal stability. Upon annealing at 160 °C

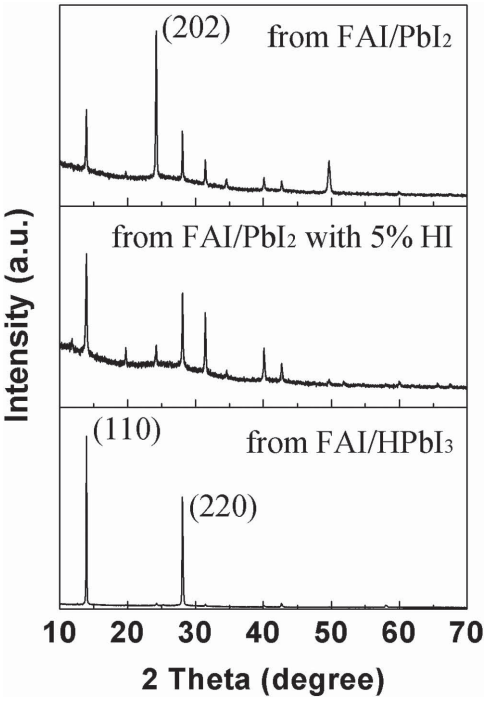

Figure 3. XRD spectra of $FAPbI_3$ films synthesized by mixing FAI with different Pb-based precursors on glass substrates.

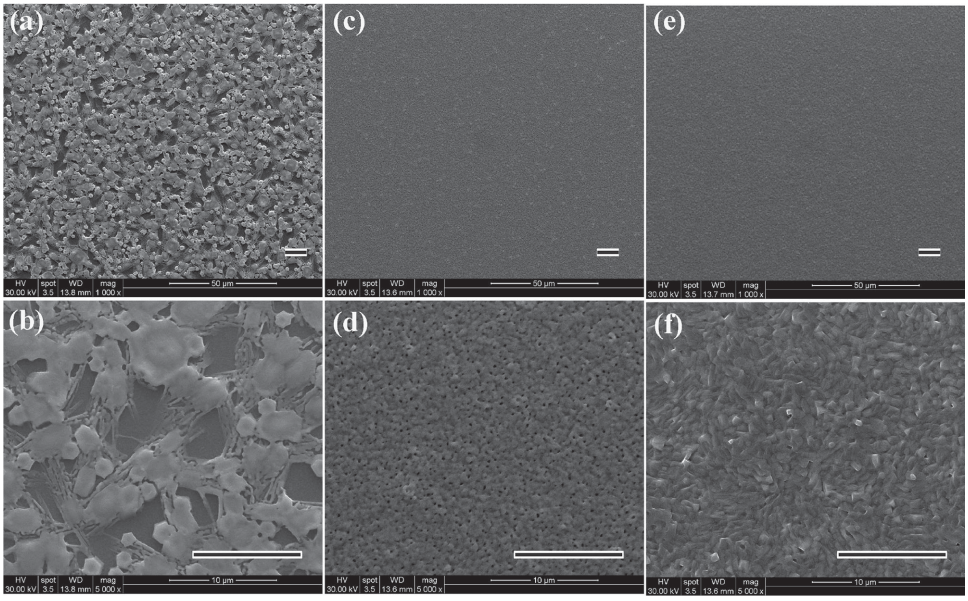

Figure 4. SEM images of $FAPbI_3$ fabricated from a,b) FAI/PbI_2, c,d) FAI/PbI_2 with 5% HI, e,f) $FAI/HPbI_3$ on compacted TiO_2 substrates. The scale bars are 10 μm.

for 80 min, the sample still exhibits pure perovskite signals in the XRD measurement (Figure S2, Supporting Information).

The morphology of the perovskite films synthesized from the three different precursor combinations were investigated by scanning electron microscopy (SEM). **Figure 4**a,b show incomplete coverage of the perovskite film formed from the FAI/PbI_2 precursor solution. In contrast, FAI/PbI_2 with 5 vol% HI additive produces uniform perovskite film that can fully cover the substrate with ≈0.4 μm grains (Figure 4c,d). The $FAPbI_3$ film formed by $FAI/HPbI_3$ is also highly uniform and compact (Figure 4e). The high-magnification SEM image of the film reveals closely packed microrods with a diameter of ≈0.3 μm and length of ≈1.5 μm (Figure 4f). It can also be seen that the voids in the $FAI/HPbI_3$ formed film are much less than those in other films. The rod-like and dense morphology in the $FAPbI_3$ film could be beneficial to the performance of photovoltaic devices.[1i,18]

2.3. Device Performance

Planar solar cells consisting of a FTO/compact TiO_2/perovskite/spiro-MeOTAD/Ag structure[6,19] were used to evaluate the photovoltaic performance of the $FAPbI_3$ perovskite films. The detailed fabrication information is described in Supporting Information. To optimize the device performance, the thickness of the $FAPbI_3$ films were tuned by varying the concentration of the precursor solution while keeping the molar ratio of FAI to $HPbI_3$ (or PbI_2) at 1:1. **Table 1** summarizes the extracted short-circuit current density (J_{sc}), open-circuit voltage (V_{oc}), and fill factor (FF) of the optimized devices. **Figure 5**a shows the effect of film thickness on the J_{sc} values for all three types of $FAPbI_3$ devices made from different precursor combinations. The optimized thickness for the $FAI/HPbI_3$ produced $FAPbI_3$ is around 330 nm, while the value is reduced to 300 nm and 260 nm for the $FAPbI_3$ films made from the FAI/PbI_2 with 5% HI and FAI/PbI_2 combinations, respectively. Interestingly, the $FAI/HPbI_3$ based perovskite solar cells exhibit an average J_{sc} of 23.8 mA cm^{-2}, surpassing the performance of the $FAPbI_3$ solar cells fabricated from FAI/PbI_2 (15.2 mA cm^{-2}) and FAI/PbI_2 with 5% HI (20.2 mA cm^{-2}). The wavelength-dependent external quantum efficiency (EQE) spectra shown in Figure 5b further confirm the current–voltage measurement results, demonstrating an improved photoresponse of the $FAI/HPbI_3$ produced perovskite solar cells over a broad spectral range (450–840 nm). The J_{sc} estimated from the EQE spectrum is ≈18.5 mA cm^{-2}, lower than the average J_{sc} obtained from the *I–V* scans of the solar cells. The J_{sc} difference can be explained by two factors: First, the onset of our EQE measurement is 400 nm, therefore the contribution from the UV portion (<400 nm) of solar radiation is not considered when estimating the J_{sc} value. Second, we note that the J_{sc} measured from an *I–V* scan is 10% higher than the one measured by directly biasing the device at 0 V. This is probably the consequence of the anomalous hysteresis and bias effect of the solar cells, which will be discussed later on.

Besides the effect of film thickness, the variation in the solar cell performance can be readily explained by the different film morphologies and crystal structures. The low J_{sc} and V_{oc} values of

Table 1. Solar cell performance of $FAPbI_3$ films produced from different precursor combinations.[a)]

Cell	J_{sc} [mA cm^{-2}]	V_{oc} [V]	FF	PCE [%]
$FAPbI_3$ (FAI/PbI_2)	15.2 ± 0.7	0.65 ± 0.05	0.45 ± 0.10	4.6 ± 1.5
$FAPbI_3$ (FAI/PbI_2 with 5% HI)	20.2 ± 0.9	0.88 ± 0.06	0.62 ± 0.08	10.9 ± 1.5
$FAPbI_3$ ($FAI/HPbI_3$)	23.8 ± 1.1	0.95 ± 0.08	0.65 ± 0.10	15.4 ± 1.7

[a)]Data for $FAPbI_3$($FAI/HPbI_3$) is averaged from 80 devices and 16 devices for others.

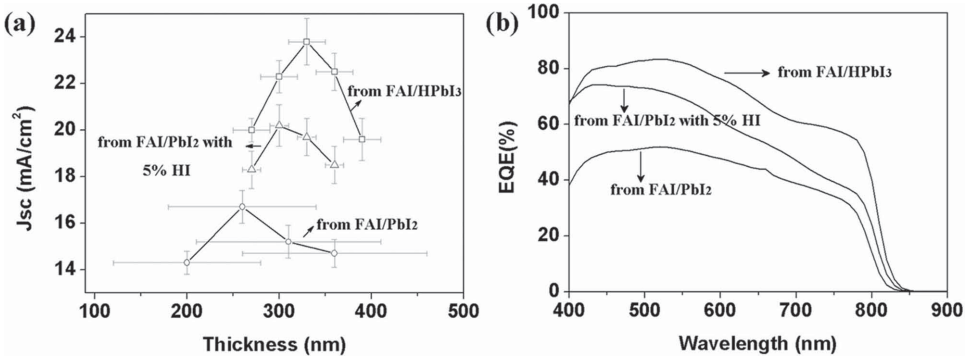

Figure 5. a) J_{sc} values of $FAPbI_3$ solar cell devices as a function of film thickness. b) External quantum efficiency (EQE) spectra of representative $FAPbI_3$ solar cell devices. The spectra are measured by biasing the device at 0 V.

the FAI/PbI_2 based solar cells are mainly due to the incomplete film coverage and large surface roughness (around 80 nm).[12,20] High leakage current and low shunt resistance are also observed for this device (Figure S4 and Table S2, Supporting Information). For FAI/PbI_2 with 5% HI and FAI/ $HPbI_3$ produced films, the size and orientation of the crystal domains may be the main factors that cause their different photoresponse. In the perovskite films formed from FAI/$HPbI_3$, the large crystal domains and (110) texture are beneficial for transport of photogenerated charge carries, leading to increased photocurrent. We also note that the average V_{oc} of the FAI/$HPbI_3$-based solar cells is slightly higher than the FAI/ PbI_2 with 5% HI based devices. From the transient photovoltage response (Figure S5, Supporting Information), we do not observe any significant difference between the two devices, which indicates that the charge recombination dynamics in the two perovskite films are similar. Therefore, we suspect that the V_{oc} difference might originate from the different Fermi-level positions in the two films.

Recently, anomalous hysteresis has been observed in the *J–V* curves of perovskite solar cells, especially in the planar-structured configuration.[21] We also recorded the *J–V* curves of the devices with different scanning directions, as well as the stabilized power output of the cells held at the maximum power point (**Figure 6**). The results show that the PCE estimated from the stabilized power output measurement is between the PCE values obtained from the forward bias (FB) to short-circuit (SC) and SC-to-FB *J–V* scans. Although such power output variation is more severe in the FAI/$HPbI_3$ produced solar cells, the devices still yield higher PCEs than the other two types of solar cells in every measurement method. A comparison of the average PCEs (estimated from FB-to-SC scans) of the three types of solar cells is provided in Table 1. The *J–V* scan of the champion FAI/$HPbI_3$ based device is shown in Figure 6c. A PCE of 17.5% is achieved at the FB-to-SC scan direction. Recent studies show that the *J–V* hysteresis could be reduced by introducing the meso-TiO_2 structures in perovskite solar cells.[10,21c,d]

3. Conclusion

In summary, we have developed a new precursor compound, $HPbI_3$, for fabrication of high efficiency perovskite solar cells via solution process. The compound shows excellent solubility (up to ≈2.5 M) in DMF at room temperature, and can react with FAI to produce $FAPbI_3$ perovskite films with high uniformity and excellent thermal stability. As compared to the previously reported $FAPbI_3$ films produced from the PbI_2 based precursor combinations, the $HPbI_3$ based $FAPbI_3$ films exhibit much purer crystalline phase with strong (110) preferred orientation. Such high crystallinity benefits from a slow crystallization process involving exchange of H^+ and FA^+ ions in the PbI_6 framework. The high quality $FAPbI_3$ films are integrated in a simple planar solar cell structure and yield an average efficiency of 15.4% and champion efficiency of 17.5% (estimated from FB-to-SC scans) under AM 1.5 illumination. The simple preparation of $HPbI_3$, together with the facial solution deposition technique, is expected to improve the reproducibility and scalability of perovskite solar cells. The versatility of the new precursor compound can be further demonstrated by the success of using (1) FAI/ $HPbI_3$ to fabricate $FAPbI_3$ perovskite on meso-porous TiO_2 substrates (Figure S6, Supporting Information), and (2) MAI/$HPbI_3$ to synthesize $MAPbI_3$ (Figure S7, Supporting Information). We therefore believe that the engineering of such precursor systems may open new possibilities to fabricate perovskite with new functionalities.

4. Experimental Section

Perovskite Precursor Synthesis: FAI powders were synthesized according to a previously reported method.[14a] Briefly, formamidinium acetate (Sigma-Aldrich, ≥98.0%) was dissolved in 57%w/w hydroiodic acid in a molar ratio of 1:2. The precipitate was recovered upon evaporating the solvent at 60 °C under reduced pressure. After washing with diethyl ether and recrystallized with ethanol, formamidinium iodide powders were obtained. $HPbI_3$ powders were prepared by mixing PbI_2 (Sigma-Aldrich, 99%) and 57%w/w hydroiodic acid (molar ratio is 1:1.5) in DMF with stirring for 1 h. The excess HI was used to ensure complete conversion of PbI_2 into $HPbI_3$. Parts of the excess HI could be removed during solvent evaporation at 80 °C under reduced pressure. The residue HI is washed by copious diethyl ether until supernatant turned to colorless. The collected powders are stored in an oven at 40 °C.

Solar Cell Fabrication: The TiO_2 compact film precursor solution in ethanol consists of 0.3 M titanium isopropoxide (Sigma-Aldrich, 99.999%) and 0.01 M HCl. An ≈40 nm dense TiO_2 film was coated onto F-doped SnO_2 (FTO) substrate by spinning titanium precursor at 5000 rpm, followed by annealing at 500 °C for 1 h. The synthesized FAI and $HPbI_3$ powders were mixed with a molar ratio of 1:1 in DMF and stirred for 10 min, and then filtered with a PTFE filter with 0.45 μm pore

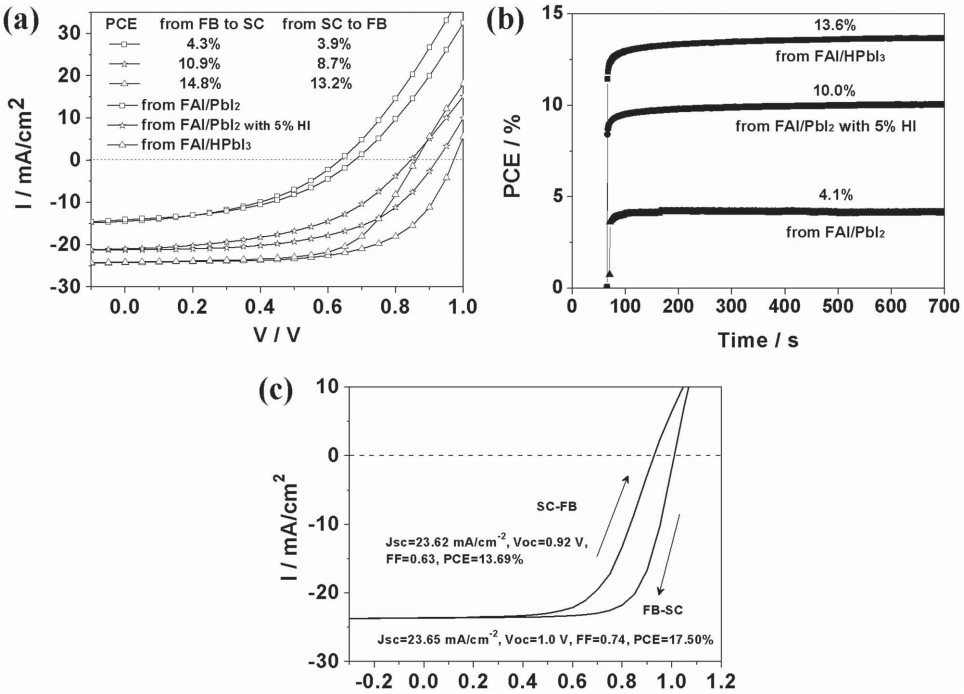

Figure 6. a) Comparison of the FB-to-SC and SC-to-FB *J–V* curves of different $FAPbI_3$ devices measured under AM 1.5 simulated sunlight. b) Stabilized power output as a function of time for the same $FAPbI_3$ devices measured in a). The cells were placed in dark for >1 min prior to the start of the illumination. See "Experimental Section" for the details of the measurement procedure. c) *J–V* curves measured under AM 1.5 simulated sunlight for the best $FAPbI_3$ device made from the $FAI/HPbI_3$ combination.

size. The precursor solution was deposited onto TiO_2/FTO substrate by spin-coating at 3000 rpm for 60 s. After drying the film on a hotplate at 130 °C for 0.5 h and 160 °C for 1.0 h, the color of the film turned from yellow to black, indicating the formation of $FAPbI_3$. The thickness of $FAPbI_3$ perovskite was controlled by varying the concentration of the precursor solution from 0.8 M–1.1 M. The highest PCE value of $FAPbI_3$ (from $FAI/HPbI_3$) was achieved from 1.0 M perovskite solution. The spiro-OMeTAD based hole-transfer layer was prepared by dissolving 60 mg spiro-OMeTAD, 30 µL lithium-bis(trifluoromethanesulfonyl) imide (Li-TFSI) solution (520 mg Li-TFSI in 1 mL acetonitrile), and 40 µL 4-tert-butylpyridine in 1 ml chlorobenzene. The devices were put into a dry cabinet for 15 h for oxidization of Spiro-OMeTAD. The hole-transfer layer was deposited by spin-coating at 5000 rpm for 30 s. Finally, a 100 nm silver layer was deposited by thermal evaporation at a pressure of 1×10^{-4} mbar. All device fabrication steps were carried out in a N_2-purged glovebox.

Measurement and Characterization: The XRD patterns of the products were recorded with a Rigaku ru-300 diffractometer using Cu $K\alpha_1$ irradiation (λ = 1.5406 Å). The general morphologies of the films were characterized by SEM (Quanta 400). The percentages of HI in $HPbI_3$ were determined by a thermogravimeteric analyzer (TGA6, Perkin-Elmer) under N_2 flow (20 mL min^{-1}) with a heating rate of 10 °C min^{-1}. Sample thicknesses were measured using an Alpha step 500 Surface profiler. The current density–voltage (*J–V*) curves were measured (Keithley Instruments, 2612 Series SourceMeter) under simulated AM 1.5 sunlight generated by a 94011A-ES Sol series Solar Simulator. The effective area of the cell was defined as 0.05 cm^2. EQE were measured with a Keithley 2400 Source Meter under monochromatic illumination generated by passing the light beam from a 250 W quartz tungsten halogen lamp into a Newport 74215 Oriel Cornerstone 260 1/4 m monochromator. A calibrated silicon diode with a known spectral response was used as a reference. The J_{sc} values were extracted from *J–V* curves under short-circuit conditions and by directly biasing the device at 0 V, respectively. For the transient photovoltage decay measurements, a white light bias was generated from a halogen lamp. A Newport LQD635-03C laser diode was used to generate transient light illumination in the devices. The anode and cathode of the device were connected across a 1 MΩ load resistor and connected to a Tektronix TDS 3014C Oscilloscope, allowing the modulated changes in the photovoltage under open circuit condition to be recorded.

Supporting Information

Supporting Information is available from the Wiley Online Library or from the author.

Acknowledgements

The authors gratefully acknowledge the fundings from Research Grants Council of Hong Kong (Grant No. T23-407/13-N), National Natural Science Foundation of China (Grant No. 61205036), and Shun Hing Institute of Advanced Engineering (Grant No. 8115041).

Received: November 12, 2014
Published online: January 7, 2015

[1] a) S. Kazim, M. K. Nazeeruddin, M. Grätzel, S. Ahmad, *Angew. Chem. Int. Ed.* **2014**, *53*, 2812; b) N. G. Park, *J. Phys. Chem. Lett.* **2013**, *4*, 2423; c) M. A. Green, A. Ho-Baillie, H. J. Snaith, *Nat. Photonics* **2014**, *8*, 506; d) T. C. Sum, N. Mathews, *Energy Environ. Sci.* **2014**, *7*, 2518; e) G. C. Xing, N. Mathews, S. Y. Sun, S. S. Lim, Y. M. Lam, M. Gratzel, S. Mhaisalkar, T. C. Sum, *Science* **2013**, *342*, 344; f) S. D. Stranks, G. E. Eperon, G. Grancini, C. Menelaou, M. J. P. Alcocer, T. Leijtens, L. M. Herz, A. Petrozza, H. J. Snaith, *Science* **2013**, *342*, 341; g) P. Gao, M. Gratzel, M. K. Nazeeruddin,

Energy Environ. Sci. **2014**, *7*, 2448; h) H. S. Kim, C. R. Lee, J. H. Im, K. B. Lee, T. Moehl, A. Marchioro, S. J. Moon, R. Humphry-Baker, J. H. Yum, J. E. Moser, M. Gratzel, N. G. Park, *Sci. Rep.* **2012**, *2*, 591; i) J. H. Heo, S. H. Im, J. H. Noh, T. N. Mandal, C.-S. Lim, J. A. Chang, Y. H. Lee, H.-J. Kim, A. Sarkar, K. NazeeruddinMd, M. Gratzel, S. I. Seok, *Nat. Photon.* **2013**, *7*, 486; j) M. M. Lee, J. Teuscher, T. Miyasaka, T. N. Murakami, H. J. Snaith, *Science* **2012**, *338*, 643.

[2] a) C. C. Stoumpos, C. D. Malliakas, M. G. Kanatzidis, *Inorg. Chem.* **2013**, *52*, 9019; b) F. Hao, C. C. Stoumpos, D. H. Cao, R. P. H. Chang, M. G. Kanatzidis, *Nat. Photonics* **2014**, *8*, 489; c) N. K. Noel, S. D. Stranks, A. Abate, C. Wehrenfennig, S. Guarnera, A.-A. Haghighirad, A. Sadhanala, G. E. Eperon, S. K. Pathak, M. B. Johnston, A. Petrozza, L. M. Herz, H. J. Snaith, *Energy Environ. Sci.* **2014**, *7*, 3061.

[3] A. Kojima, K. Teshima, Y. Shirai, T. Miyasaka, *J. Am. Chem. Soc.* **2009**, *131*, 6050.

[4] Q. Chen, H. Zhou, Z. Hong, S. Luo, H.-S. Duan, H.-H. Wang, Y. Liu, G. Li, Y. Yang, *J. Am. Chem. Soc.* **2013**, *136*, 622.

[5] a) J. Burschka, N. Pellet, S. J. Moon, R. Humphry-Baker, P. Gao, M. K. Nazeeruddin, M. Gratzel, *Nature (London)* **2013**, *499*, 316; b) K. N. Liang, D. B. Mitzi, M. T. Prikas, *Chem. Mater.* **1998**, *10*, 403.

[6] M. Z. Liu, M. B. Johnston, H. J. Snaith, *Nature* **2013**, *501*, 395.

[7] M. Graetzel, R. A. J. Janssen, D. B. Mitzi, E. H. Sargent, *Nature* **2012**, *488*, 304.

[8] H. Yu, F. Wang, F. Xie, W. Li, J. Chen, N. Zhao, *Adv. Funct. Mater.* **2014**, *24*, 7102.

[9] P. Docampo, F. Hanusch, S. D. Stranks, M. Döblinger, J. M. Feckl, M. Ehrensperger, N. K. Minar, M. B. Johnston, H. J. Snaith, T. Bein, *Adv. Energy Mater.* **2014**,*4*, DOI: 10.1002/aenm.201400355.

[10] N. J. Jeon, J. H. Noh, Y. C. Kim, W. S. Yang, S. Ryu, S. I. Seok, *Nat. Mater.* **2014**, *13*, 897.

[11] Y. Wu, A. Islam, X. Yang, C. Qin, J. Liu, K. Zhang, W. Peng, L. Han, *Energy Environ. Sci.* **2014**, *7*, 2934.

[12] M. Xiao, F. Huang, W. Huang, Y. Dkhissi, Y. Zhu, J. Etheridge, A. Gray-Weale, U. Bach, Y.-B. Cheng, L. Spiccia, *Angew. Chem. Int. Ed.* **2014**, *53*, 9898.

[13] P.-W. Liang, C.-Y. Liao, C.-C. Chueh, F. Zuo, S. T. Williams, X.-K. Xin, J. Lin, A. K. Y. Jen, *Adv. Mater.* **2014**, *26*, 3748.

[14] a) G. E. Eperon, S. D. Stranks, C. Menelaou, M. B. Johnston, L. M. Herz, H. J. Snaith, *Energy Environ. Sci.* **2014**, *7*, 982; b) N. Pellet, P. Gao, G. Gregori, T. Y. Yang, M. K. Nazeeruddin, J. Maier, M. Gratzel, *Angew. Chem. Int. Ed.* **2014**, *53*, 3151; c) J.-W. Lee, D.-J. Seol, A.-N. Cho, N.-G. Park, *Adv. Mater.* **2014**, *26*, 4991.

[15] a) A. Cortel, *J. Chem. Educ.* **1997**, *74*, 297; b) I. Delgery, *C. R. Hebd. Séances Acad. Sci.* **1947**, *224*, 915; c) L. Roger, *Ann. Chim. Appl.* **1944**, *19*, 362; d) O. N. Yunakova, V. K. Miloslavskii, E. N. Kovalenko, *Adv. Funct. Mater.* **2013**, *20*, 59; e) V. F. Mironov, *Synthetic Studies in the Field of Organic Germanium Compounds*, Harwood Academic Publishers GmbH, UK **1989**.

[16] P. A. Beckmann, *Cryst. Res. Technol.* **2010**, *45*, 455.

[17] D. B. Mitzi, *Prog. Inorg. Chem.* **1999**, *48*, 1.

[18] G. E. Eperon, V. M. Burlakov, P. Docampo, A. Goriely, H. J. Snaith, *Adv. Funct. Mater.* **2014**, *24*, 151.

[19] P. Docampo, J. M. Ball, M. Darwich, G. E. Eperon, H. J. Snaith, *Nat. Commun.* **2013**, *4* , DOI: 10.1038/Ncomms3761.

[20] Q. Wang, Y. Shao, Q. Dong, Z. Xiao, Y. Yuan, J. Huang, *Energy Environ. Sci.* **2014**, *7*, 2359.

[21] a) H. J. Snaith, A. Abate, J. M. Ball, G. E. Eperon, T. Leijtens, N. K. Noel, S. D. Stranks, J. T. W. Wang, K. Wojciechowski, W. Zhang, *J. Phys. Chem. Lett.* **2014**, *5*, 1511; b) H. P. Zhou, Q. Chen, G. Li, S. Luo, T. B. Song, H. S. Duan, Z. R. Hong, J. B. You, Y. S. Liu, Y. Yang, *Science* **2014**, *345*, 542; c) E. L. Unger, E. T. Hoke, C. D. Bailie, W. H. Nguyen, A. R. Bowring, T. Heumuller, M. G. Christoforo, M. D. McGehee, *Energy Environ. Sci.* **2014**, *7*, 3690; d) H. S. Jung, N.-G. Park, *Small* **2014**, DOI: 10.1002/smll.201402767; e) H.-S. Kim, N.-G. Park, *Phys. Chem. Lett.* **2014**, *5*, 2927.